Journal Club do Laboratório de Física Atmosférica
Departamento de Física Aplicada

Alex Sandro Alves de Araujo
Orientador: Prof. Dr. Henrique de Melo Jorge Barbosa

Instituto de Física da USP - IFUSP

alex.fate2000@gmail.com

16 de maio de 2018

Trabalho a ser apresentado

PNAS

Rainforest-initiated wet season onset over the southern Amazon

Jonathon S. Wright[a], Rong Fu[b,1], John R. Worden[c], Sudip Chakraborty[b], Nicholas E. Clinton[d], Camille Risi[e], Ying Sun[c,2], and Lei Yin[f]

[a]Department of Earth System Science, Tsinghua University, Beijing 100084, China; [b]Department of Atmospheric and Oceanic Sciences, University of California, Los Angeles, CA 90095; [c]Jet Propulsion Laboratory, California Institute of Technology, Pasadena, CA 91109; [d]Geo for Good, Google, Inc., Mountain View, CA 94043; [e]Laboratoire de Météorologie Dynamique, Institut Pierre Simon Laplace, 75252 Paris, France; and [f]Jackson School of Geosciences, University of Texas at Austin, Austin, TX 78712

Edited by Mark H. Thiemens, University of California at San Diego, La Jolla, CA, and approved June 14, 2017 (received for review January 3, 2017)

Although it is well established that transpiration contributes much of the water for rainfall over Amazonia, it remains unclear whether transpiration helps to drive or merely responds to the seasonal cycle of rainfall. Here, we use multiple independent satellite datasets to show that rainforest transpiration enables an increase of shallow convection that moistens and destabilizes the atmosphere during the initial stages of the dry-to-wet season transition. This shallow convection moisture pump (SCMP) preconditions the atmosphere at the regional scale for a rapid increase in rain-bearing deep convection, which in turn drives moisture convergence and wet season onset 2–3 mo before the arrival of the Intertropical Convergence Zone (ITCZ). Aerosols produced by late dry season biomass burning may alter the efficiency of the SCMP. Our results highlight the mechanisms by which interactions among land surface processes, atmospheric convection, and biomass burning may alter the timing of wet season onset and provide a mechanistic framework for understanding how defor-

late dry season increases in rainforest transpiration may increase surface air humidity and buoyancy (18, 19). Lifting of this humid near-surface air by cold fronts moving northward from midlatitude South America (20) could cause large-scale increases in deep convection and upper-level heating (21), thereby initiating moisture transport from the tropical Atlantic. Large-scale moisture transport reinforces the conditions that favor deep convection, ultimately leading to wet season onset. We refer to this transition mechanism as the deep convective moisture pump (DCMP).

The exact processes that activate the DCMP have been unclear. Cold front incursions are strongest during the dry season (22), but deep convection is rare until lower tropospheric humidity rises late in the transition season (21). Moistening of the lowest 4 km of the atmosphere (pressures $\gtrsim$600–700 hPa) therefore emerges as the likely key to activating the DCMP (23, 24). The source of this moisture and the processes by which moistening occurs have profound implications for understanding how land

Estrutura da apresentação

- Introdução
- Estágios de transição
- Composição isotópica
- Convecção rasa
- Implicações

Questões e fatos

- A região estudada foi o sul da Amazônia.

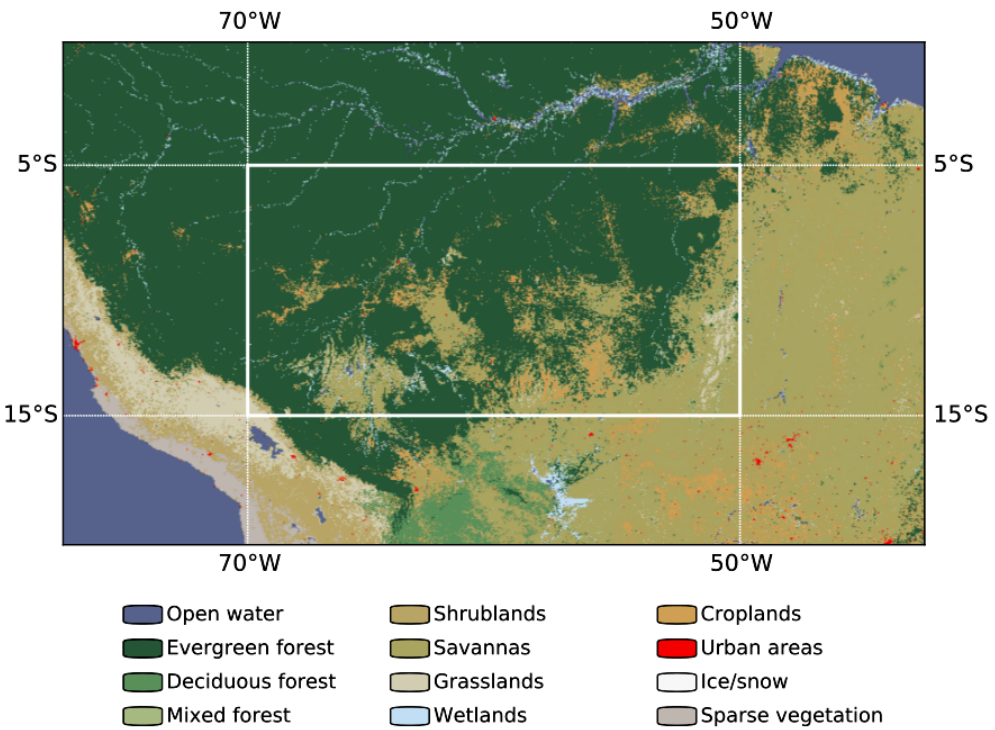

Fig. 1. Distribution of land cover based on Moderate-Resolution Imaging Spectroradiometer observations from 2009. The southern Amazon (5°S to 15°S, 50°W to 70°W) is indicated by the solid white box.

- O sul ($30 - 40$ %) da Amazônia é transição entre floresta tropical (N e W) e savana subtropical e terras de agricultura (S e E).
- Vulnerável a pequenas diminuições na chuva anual ou extensões temporais da seca.
- A seca na região tem aumentado nas últimas décadas, principalmente devido ao atraso das chuvas.

Principal questão:

- A evapotranspiração da floresta é responsável por $\approx 30 - 50$ % da chuva regional, **mas ainda é obscuro se essa evapotranspiração ativamente modifica ou simplesmente responde à sazonalidade das chuvas na Amazônia.**

Mecanismo de bombeamento de umidade

Deep Convection Moisture Pump DCMP

• O começo da temporada chuvosa nos trópicos geralmente está associado seja **(1)** à reversão nos gradientes de temperatura (terra-oceano) ou **(2)** à migração (norte-sul) da Zona de Convergência Intertropical (ZCI).

• Para o sul da Amazônia, entretanto, **a temporada chuvosa precede em 2 a 3 meses a migração da ZCI em direção ao sul, ocorrendo sem a reversão do gradiente de temperatura (terra-oceano).** Portanto, mecanismos convencionais não explicam o começo das chuvas nessa região.

• **Mecanismos envolvidos numa hipótese alternativa:**

1. Ocorrem aumentos da transpiração da floresta no final da temporada seca que leva a um aumento da umidade e flutuabilidade do ar (fato).
2. A elevação desse ar úmido da superfície pelas frentes frias vindas do sul poderiam aumentar a convecção profunda e o aquecimento dos níveis mais altos, iniciando assim o transporte de umidade do Oceano Atlântico.
3. Esse transporte de larga escala de umidade retroalimentaria as condições que favorecem a convecção profunda, o que por sua vez levaria ao início da temporada chuvosa. Tal mecanismo é chamado de *Deep Convection Moisture Pump (DCMP)*.

Mecanismo de bombeamento de umidade

Deep Convection Moisture Pump DCMP

• Alguns problemas envolvidos com o mecanismo anterior: **(1)** o exato processo que ativa esse bombeamento não está claro e **(2)** as incursões das frentes frias são mais fortes durante a temporada seca, mas convecção profunda é rara até que a baixa troposfera se torne úmida, o que por sua vez ocorre no final da estação de transição.

• Dessa forma, a umidificação dos 4 km mais baixos da atmosfera ($p > \approx 600-700$hPa) emerge como um ingrediente chave na ativação da *DCMP*.

• **Questão importante:** o aumento da umidade no final da temporada seca vem da transpiração da floresta ou vem da advecção do oceano?

• Estudos anteriores a esse respeito tem sido majoritariamente baseados em produtos de reanálises (observações + modelos). **Problemas para representar o transporte de umidade na Amazônia:** por exemplo, o aumento da precipitação durante a temporada de transição ocorre de 2 a 3 semanas antes no *European Center for Medium-Range Weather Forecasting Interim Reanalysis (ERA-Interim)*, em relação aos dados observados.

• Os produtos de reanálise têm dificuldades de atribuir as fontes de umidade: *evapotranspiration (ET)* ou *moisture flux convergence (MFC)*

• As observações *in situ* indicam que o máximo de evapotranspiração leva ao aumento das chuvas no final da temporada seca. Entretanto, não se sabe de aumentos modestos na evapotranspiração podem contribuir significativamente com umidade acima da camada limite em escala regional.

• Além disso, **a maioria dos produtos de reanálise não levam em consideração ou subestimam as variações sazonais e interanuais de aerossol.**

Seca - chuvosa

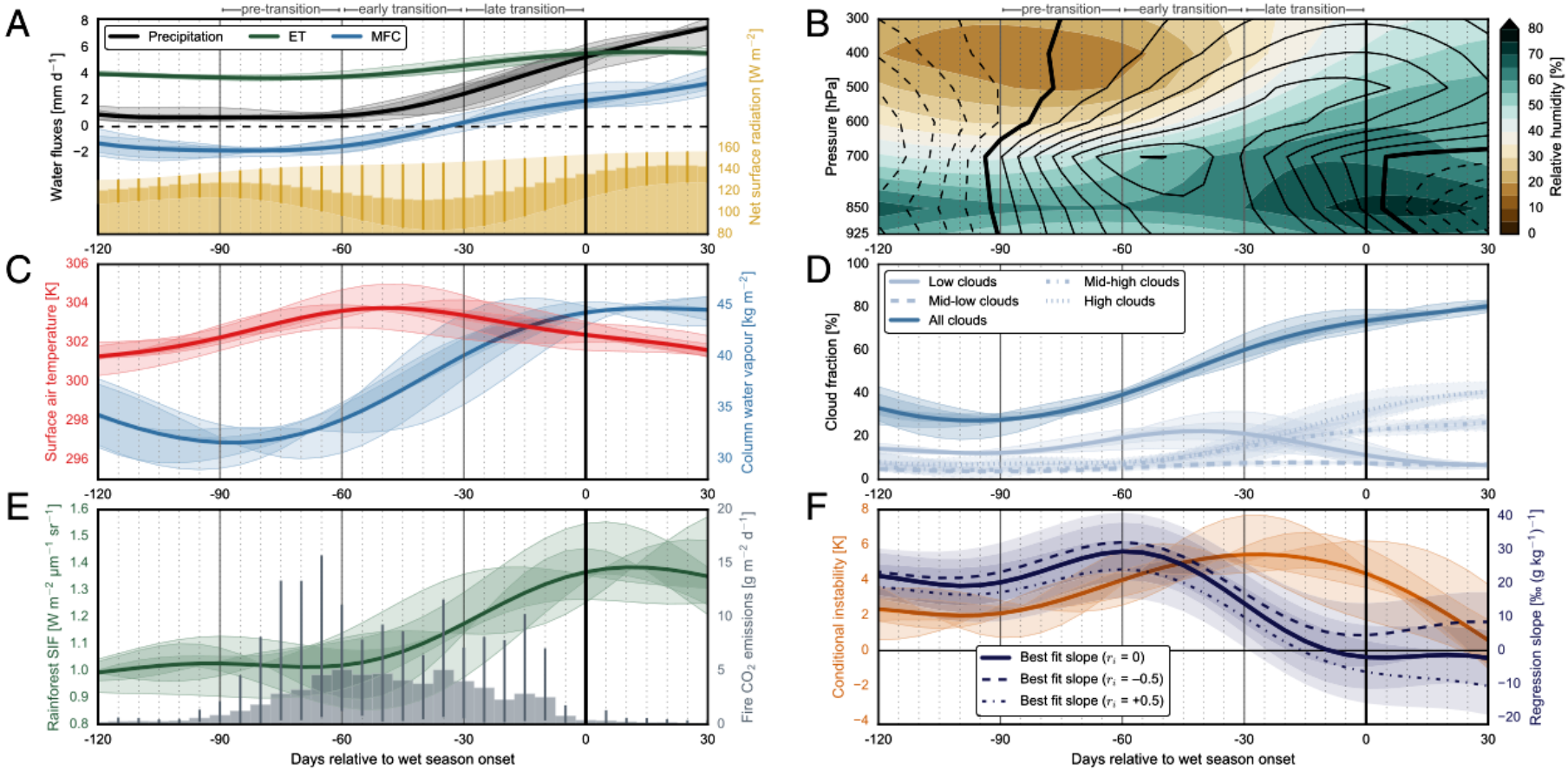

Fig. 2. Onset-relative low-pass filtered composites of area mean precipitation from Tropical Rainfall Measuring Mission (TRMM), ET and MFC from ERA-Interim, and net absorbed surface radiation from Clouds and the Earth's Radiant Energy System (CERES) Synoptic Radiative Fluxes and Clouds (SYN1Deg) (*A*); vertical distributions of RH (shading) and time rates of change in equivalent potential temperature ($\partial\theta_e/\partial t$; contour interval 0.02 K d^{-1}) computed from Atmospheric Infrared Sounder (AIRS) observations (*B*); surface air temperature and column water vapor (CWV) from AIRS (*C*); low (<700 hPa; ∼3 km above sea level), midlow (700–500 hPa; ∼3–5.5 km), midhigh (500–300 hPa; ∼5.5–10 km), high (>300 hPa; ∼10 km), and total cloud cover from CERES SYN1deg (*D*); solar-induced chlorophyll fluorescence (SIF) for rainforests from the Global Ozone Monitoring Instrument 2 and fire emissions of CO_2 from Version 3.1 of the Global Fire Emissions Database (*E*); conditional instability in the lower–middle troposphere ($\theta_{e850} - \theta_{e500}$) based on AIRS and best-fit linear slopes of δD against specific humidity (q) in the free troposphere based on TES (*F*). Shaded areas in *A* and *C*–*F* and error bars in *A* and *E* illustrate estimated uncertainties. Data sources, quality control criteria, and uncertainty calculations are provided in *SI Text*.

Isótopos

• As análises anteriores de evapotranspiração (ET) e de umidade (MFC) são baseadas em produtos de reanálise. A análise foi suplementada estudando-se a composição istópica do vapor de água.

• As diferenças moleculares entre os isótopos H2O e HDO causam fracionamento durante a maioria das transições de fase: O isótopo mais pesado HDO **preferencialmente condensa**, enquanto que o mais leve H2O **preferencialmente evapora**.

• **A evaporação do oceano em conjunto com a condensação durante o transporte diminuem o deutério do vapor de água em relação à sua origem. Em contraste, não ocorre fracionamento durante a transpiração, de modo que a composição isotópica do vapor é virtualmente idêntica à da água do solo.**

• O conteúdo de deutério δD da amostra de vapor é dado em partes por mil $‰$:

$$\delta D = 1000 \cdot \left[\frac{\frac{N_{HDO}}{N_{H_2O}} - \left(\frac{N_{HDO}}{N_{HDO}}\right)_{STD}}{\left(\frac{N_{HDO}}{N_{H_2O}}\right)_{STD}} \right] \tag{1}$$

onde N_{HDO} e N_{H2O} são as concentrações dos respectivos isótopos, e o subscrito STD se refere ao padrão de Viena:

$$\left(\frac{N_{HDO}}{N_{H2O}}\right)_{STD} = 3,11 \cdot 10^{-4}$$

Isótopos

• Em condições recorrentes, observa-se diferenças na composição isotópicas dos vapores de água:

$$\delta D_{\text{oceano}} \approx -70 \text{ a } -80‰; \qquad \delta D_{\text{evapotranspiração}} \approx -20 \text{ a } -40‰ \tag{2}$$

Dessa forma, pode-se tratar a evaporação do oceano e a evapotranspiração da floresta como **fontes de umidade isotopicamente distintas**, sendo a evapotranspiração da floresta mais enriquecida com deutério.

• Disto isto, se as umidades maiores na troposfera livre ($\approx 750 - 348\,\text{hPa}$) forem mais enriquecidas com deutério, então essa umidade está associada com a evapotranspiração da floresta e, caso contrário, com o oceano.

• Com isso, pode-se analisar o ajuste linear δD contra q, sendo que as maiores inclinações estão relacionadas com umidade vinda da evapotranspiração, e as menores inclinações com a umidade do Oceano.

Resultados

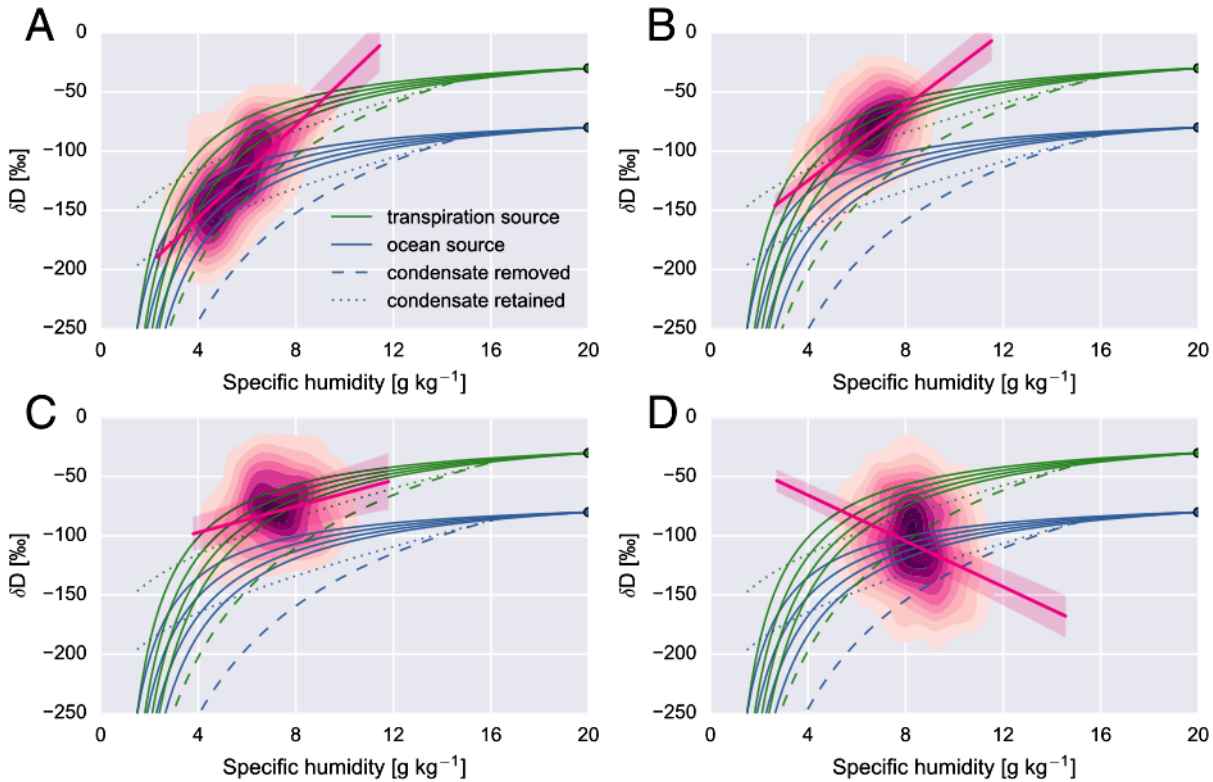

Fig. 3. Joint distributions of specific humidity (q) and the deuterium content of water vapor (δD) in the lower troposphere (825–600 hPa) based on TES observations during the pretransition stage (day −90 to −60) (*A*), early transition (day −60 to −30) (*B*), late transition (day −30 to 0) (*C*), and the first 3 mo of the wet season (day 0 to +90) (*D*). The joint behaviors of q and δD under three types of idealized vertical mixing are also shown. Solid green and blue lines represent mixing (no condensation) between four dry air masses representing the dry season free troposphere and a moist air mass representing either local ET (green; $q = 20$ g kg^{-1}; δD = −30‰) or ocean evaporation (blue; $q = 20$ g kg^{-1}; δD = −80‰). Dashed green and blue lines represent pseudoadiabatic Rayleigh distillation from the approximate top of the ABL, in which condensation occurs in a rising air parcel and is immediately removed as precipitation. Dotted green and blue lines represent reversible moist adiabatic ascent from the approximate top of the ABL, in which condensation occurs and is assumed to remain in the parcel. These idealized models are described in detail in *SI Text*.

Resultados

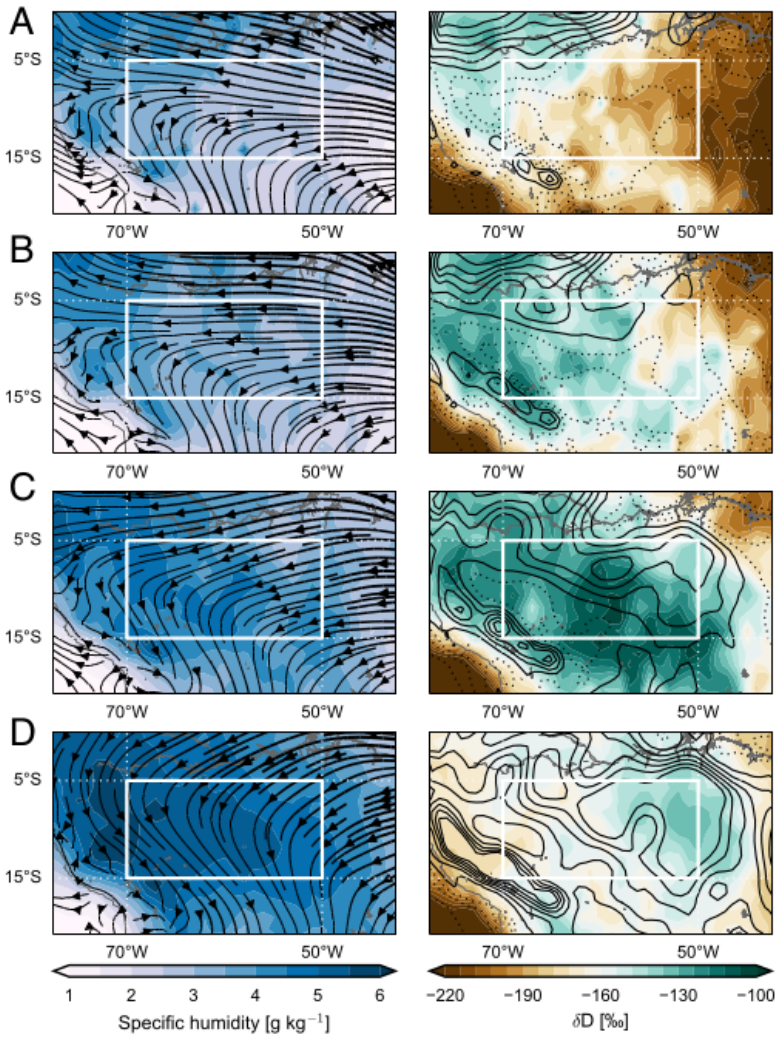

Fig. 4. Distribution of specific humidity (*Left*) and δD (*Right*) in the free troposphere based on TES observations during the pretransition (day −90 to −60) (*A*), early transition (day −60 to −30) (*B*), late transition (day −30 to 0) (*C*), and early wet season (day 0 to +90) (*D*). Winds at 850 hPa (*Left*) and vertically integrated MFC (*Right*) based on ERA-Interim are also shown for each stage of the transition. The contour interval for MFC is 1 kg m^{-2} d^{-1}.

Influência do aerossol

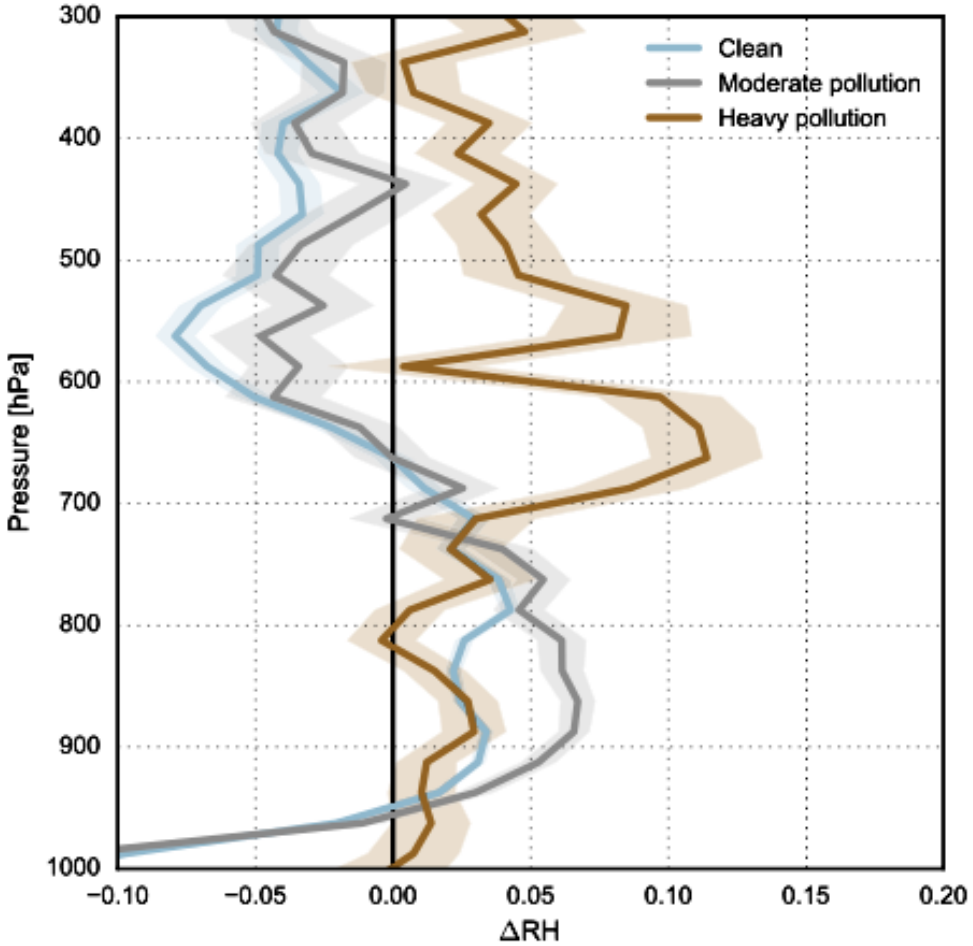

Fig. 5. Changes in the vertical profiles of RH (ΔRH) associated with shallow convection under clean conditions [Cloud condensation number concentrations (CCN) ≤ 500 cm^{-3}], moderate aerosol pollution (500 cm^{-3} $<$ CCN $\leq 1{,}000$ cm^{-3}), and heavy aerosol pollution (CCN $> 1{,}000$ cm^{-3}). CCN, RH profiles, and convective occurrence are based on observations collected during the Green Ocean Amazon (GOAmazon) field campaign (*SI Text*). ΔRH is reported in absolute differences.

Conclusões e comentários

• Sabe-se que o destino da floresta no sul da Amazônia depende da extensão temporal da temporada seca. Os autores mostraram que a extensão da temporada seca também depende da floresta.

• A evapotranspiração da floresta no final da temporada seca ajuda a iniciar um cascata de processos atmosféricos que aceleram o início da temporada chuvosa 2 a 3 meses antes da chegada da ZCI. **Esses resultados reforçam a hipótese de que o desflorestamento pode atrasar o início das chuvas da temporada úmida a estender o período de seca.**

• Muitos modelos ainda permanecem incapazes de reproduzir realisticamente a evapotranspiração da floresta e a convecção rasa, **levando a erros em relação aos mecanismos que controlam as chuvas na Amazônia e grandes discrepâncias quanto às mudanças climáticas projetadas no sul da Amazônia.**

• O começo da temporada chuvosa iniciado pela evapotranspiração também pode-se aplicar para outras regiões da Amazônia, mas são necessários mais estudos para se avaliar essa possibilidade.

FIM

OBRIGADO !

Materiais e métodos

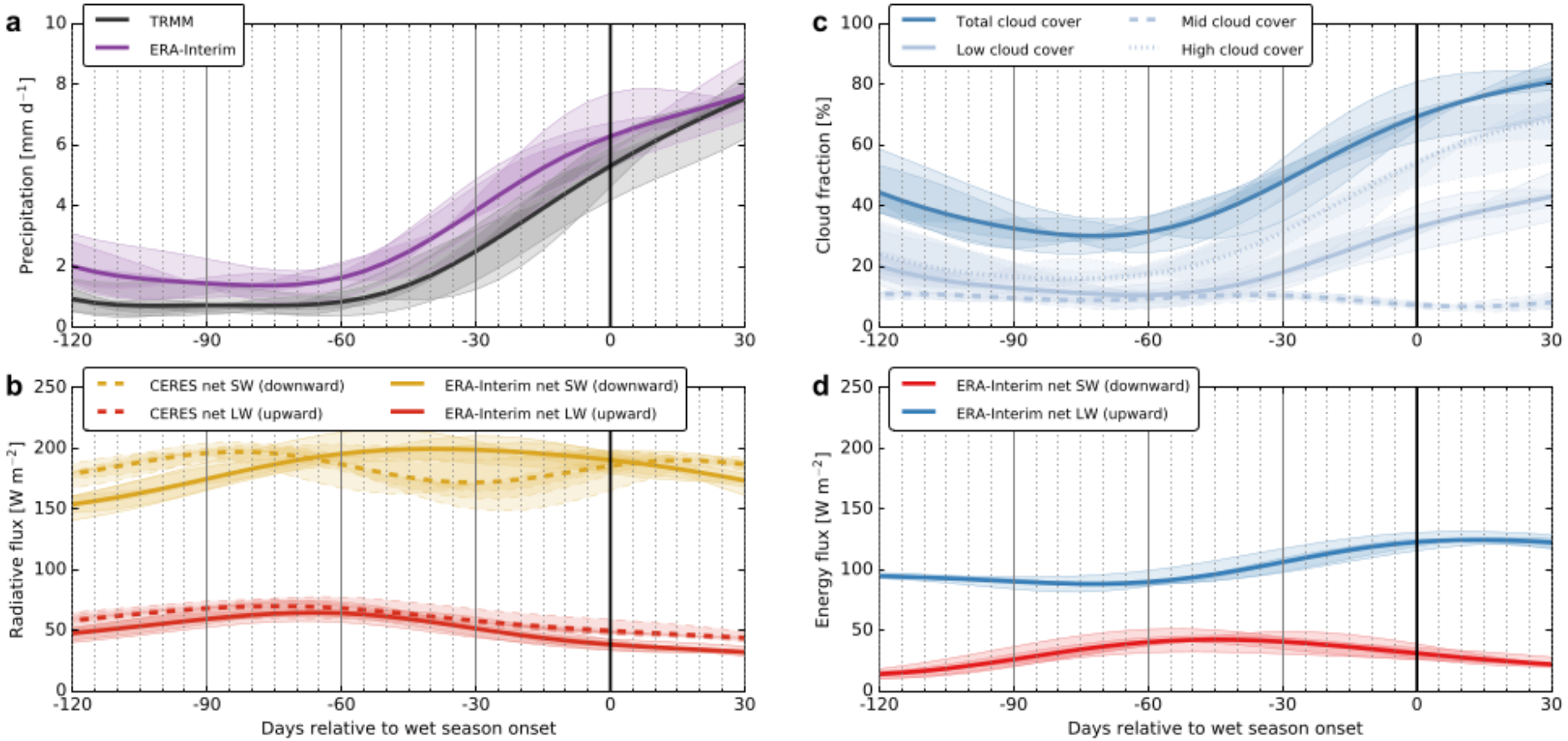

Fig. S1. Onset-relative time series of precipitation from TRMM and ERA-Interim (*A*), net fluxes of shortwave (downward) and longwave (upward) radiation at the surface from ERA-Interim and CERES SYN1Deg (*B*), cloud fraction from ERA-Interim (*C*), and upward sensible and latent heat fluxes from ERA-Interim (*D*). All fluxes represent area-weighted averages over the southern Amazon region during the period 2005–2011. Uncertainties represent interannual variability across six dry-to-wet transition seasons.

Materiais e métodos

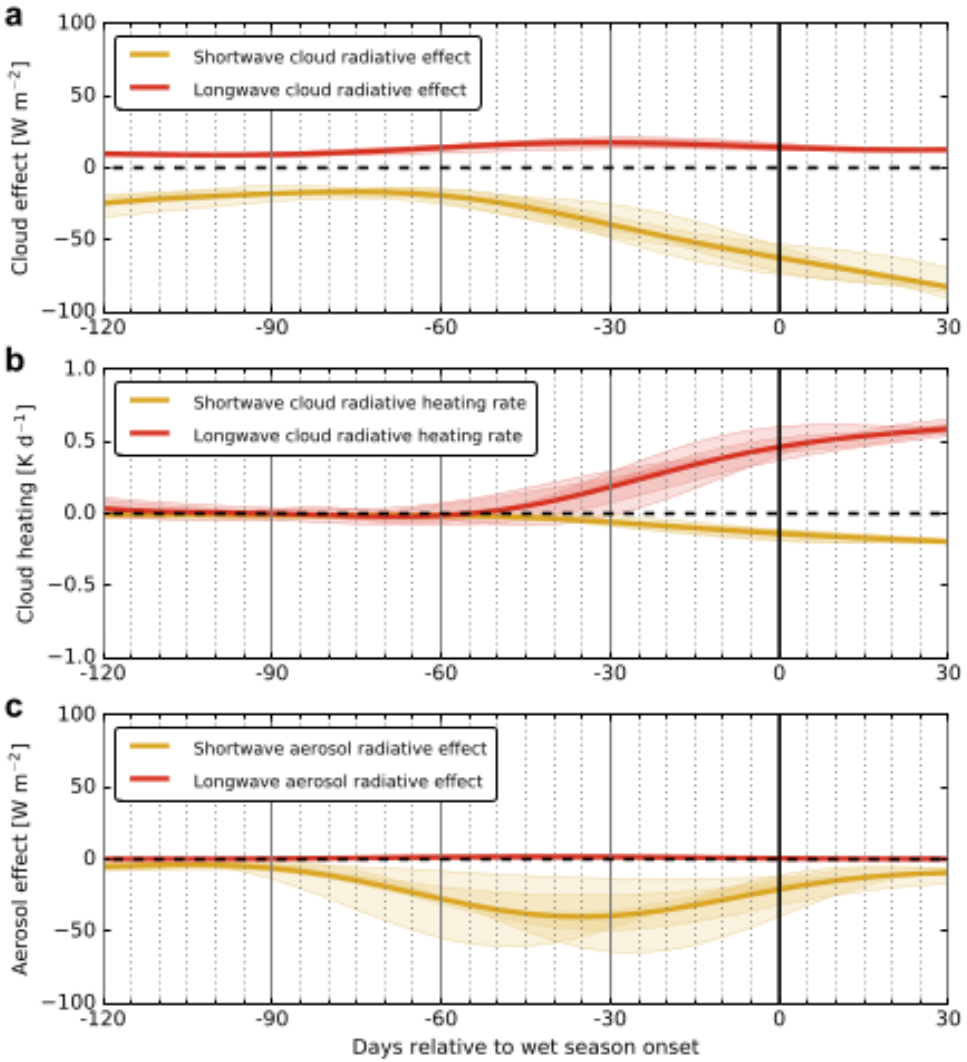

Fig. S2. Onset-relative time series of cloud radiative effect on net downward shortwave and longwave radiation at the surface (*A*), cloud radiative heating due to shortwave and longwave radiation between the surface and 500 hPa (assuming a mean surface pressure of 1,000 hPa and a dry atmosphere in hydrostatic balance) (*B*), and aerosol radiative effect on net downward shortwave and longwave radiation at the surface (*C*). All variables are calculated from CERES SYN1Deg data. Uncertainties represent interannual variability across six dry-to-wet transition seasons.

Materiais e métodos

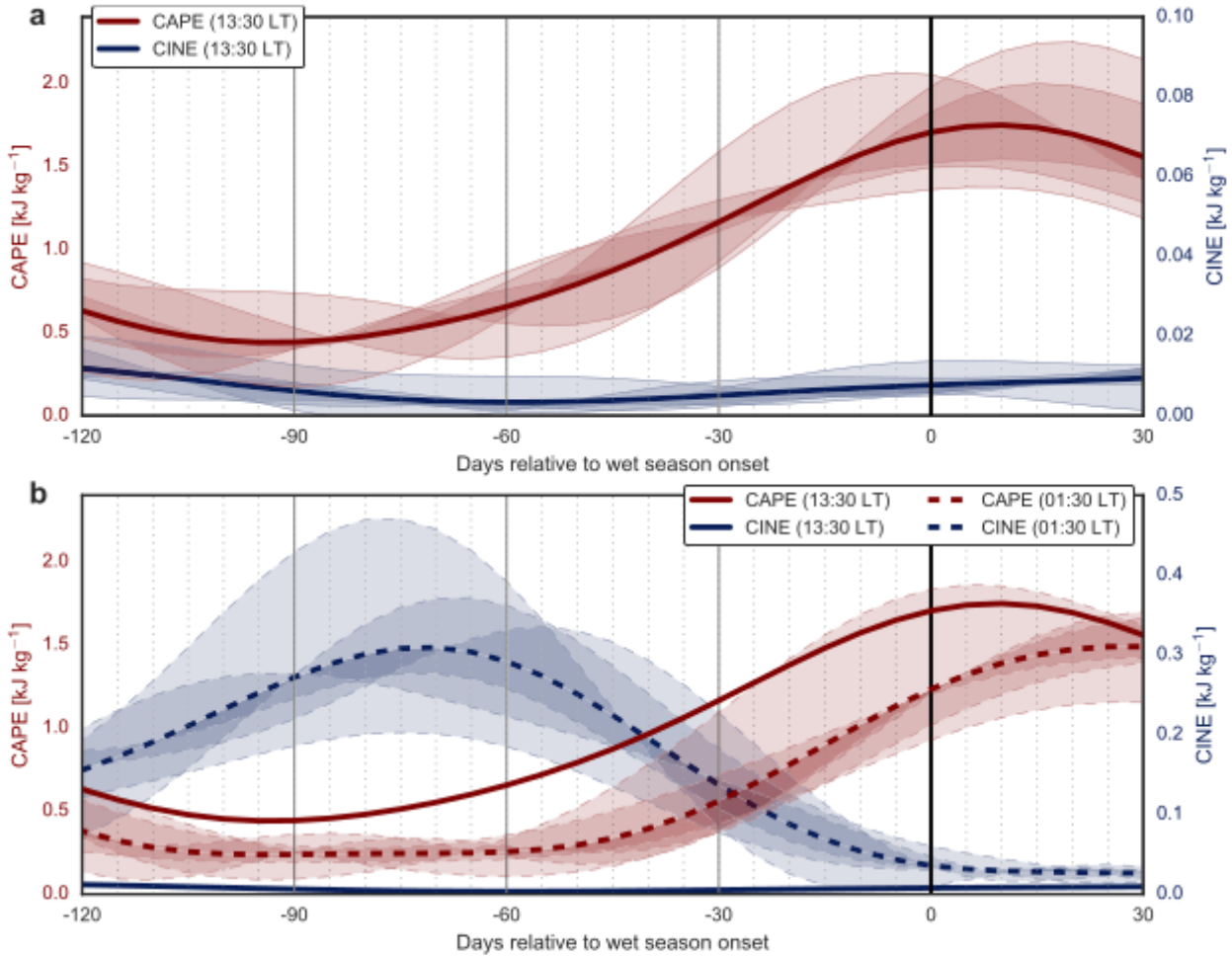

Fig. S3. Onset-relative composite time series of area-weighted 5-d mean CAPE (red lines) and CINE (blue lines) calculated from daily 1° × 1° AIRS profiles of temperature and water vapor during ascending (daytime) (*A*) and descending (nighttime) (*B*) orbits. Larger values of CAPE indicate greater convective instability, whereas larger values of CINE indicate a larger energetic barrier to convection. Note different ranges of the CINE axis between *A* and *B*. Mean evolution of daytime values are shown in *B* to facilitate comparison. Uncertainties represent interannual variability across six dry-to-wet transition seasons.

Materiais e métodos

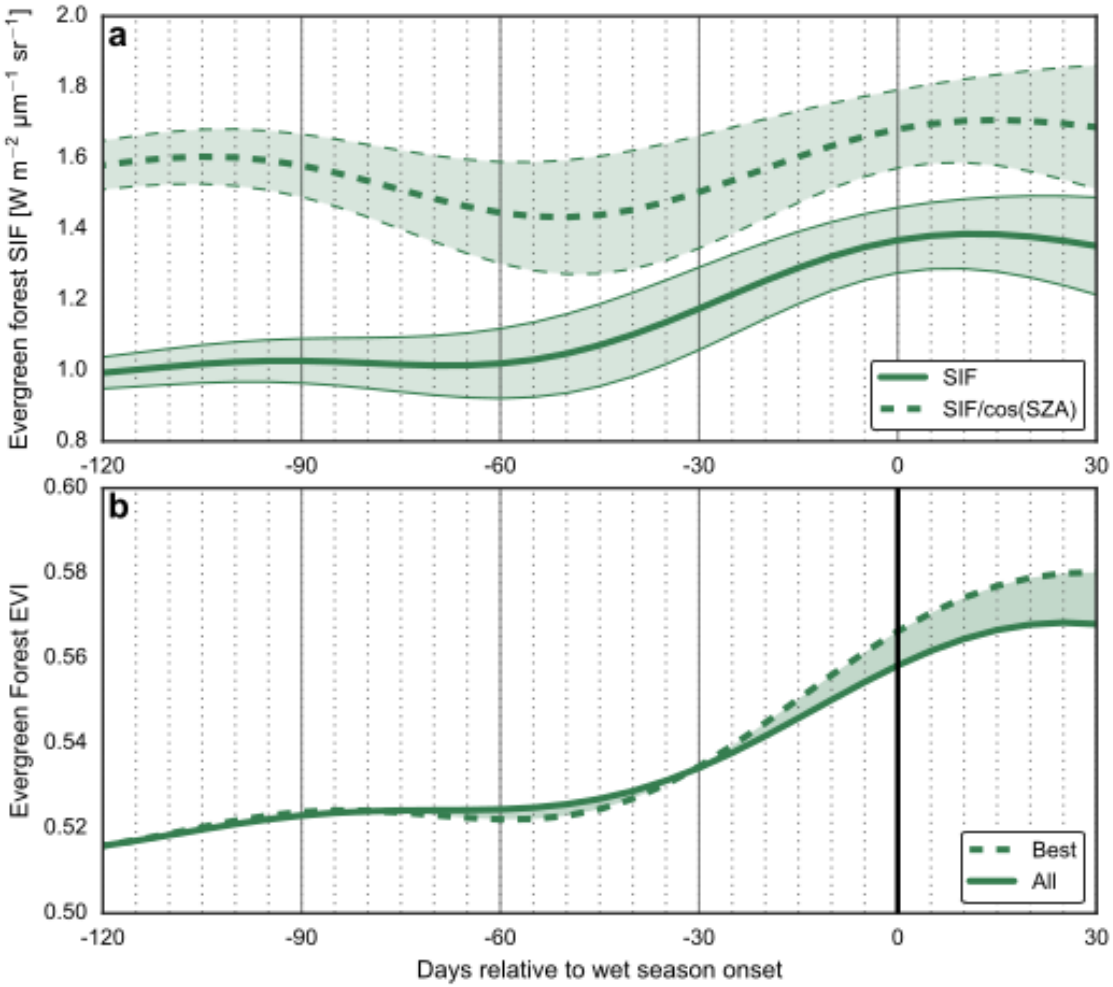

Fig. S4. Onset-relative time series of SIF from GOME-2 observations (*A*) and EVI calculated from MODIS observations (*B*). Two variations of SIF are shown, both covering the time period 2007–2014. The raw SIF data (solid line) are identical to those shown in Fig. 2*E*. SIF normalized by the cosine of the solar zenith angle (dashed line) is also shown for context and comparison with EVI. Uncertainty windows in both SIF estimates reflect interannual variability quantified as SDs across seven dry-to-wet transition seasons. The EVI data cover the time period 2005–2011, consistent with all non-SIF data shown in Fig. 2. Again, two variations are shown, one based on strict quality control standards (dashed) and one based on minimum quality control standards (solid; see *SI Text, Vegetation Metrics and Fire Emissions* for details). On average, late dry season increases in EVI lag late dry season increases in SIF by 10 ∼ 15 d.

Materiais e métodos

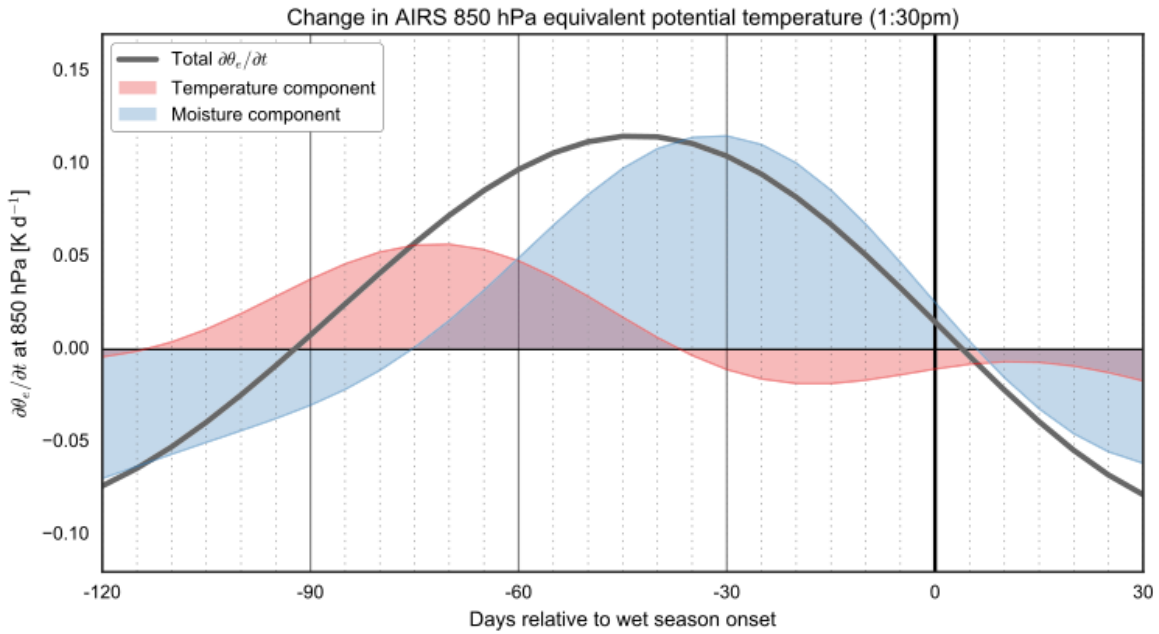

Fig. S5. Onset-relative composite time series of temperature (red shading) and moisture (blue shading) contributions to the time rate of change in θ_e (thick gray line) at 850 hPa based on AIRS observations. Temperature and moisture contributions are calculated following Li and Fu (19).

Materiais e métodos

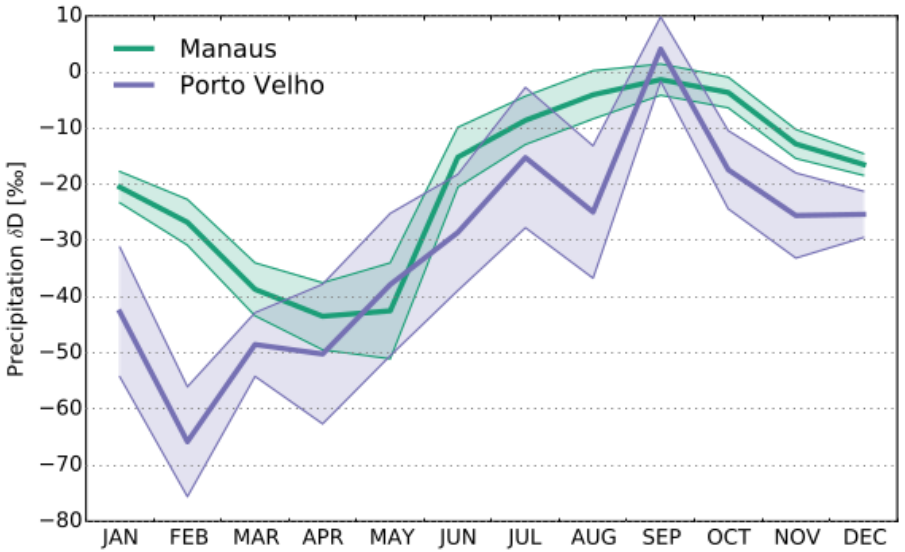

Fig. S6. Annual variability of monthly mean δD in precipitation according to samples collected at Porto Velho (8.77°S, 63.92°W) and Manaus (3.12°S, 60.02°W) under the Global Network for Isotopes in Precipitation (GNIP) measurement program. Data at Porto Velho were collected sporadically between 1965 and 1981, with the sample sizes ranging from four (July and August) to nine (November). Data at Manaus were collected sporadically between 1965 and 1990, with sample sizes ranging from 10 (September) to 17 (December). Effectively zero fractionation occurs during rainforest transpiration (34). δD in transpired water vapor should therefore approximately match δD in soil water; lacking direct observations, we estimate this as the precipitation-weighted mean δD in rainfall. The precipitation-weighted mean δD based on these data are approximately $-38‰$ at Porto Velho and $-26‰$ at Manaus. Previous studies suggest that this should represent a lower bound on δD in soil water, because the isotopic content of bound water accessed by tree roots in ecosystems with clearly delineated dry and wet seasons is weighted toward that of rainfall during the dry and transition seasons, when rain rates are lower and runoff fractions are smaller (70). GNIP data can be accessed at www.iaea.org/water.

Materiais e métodos

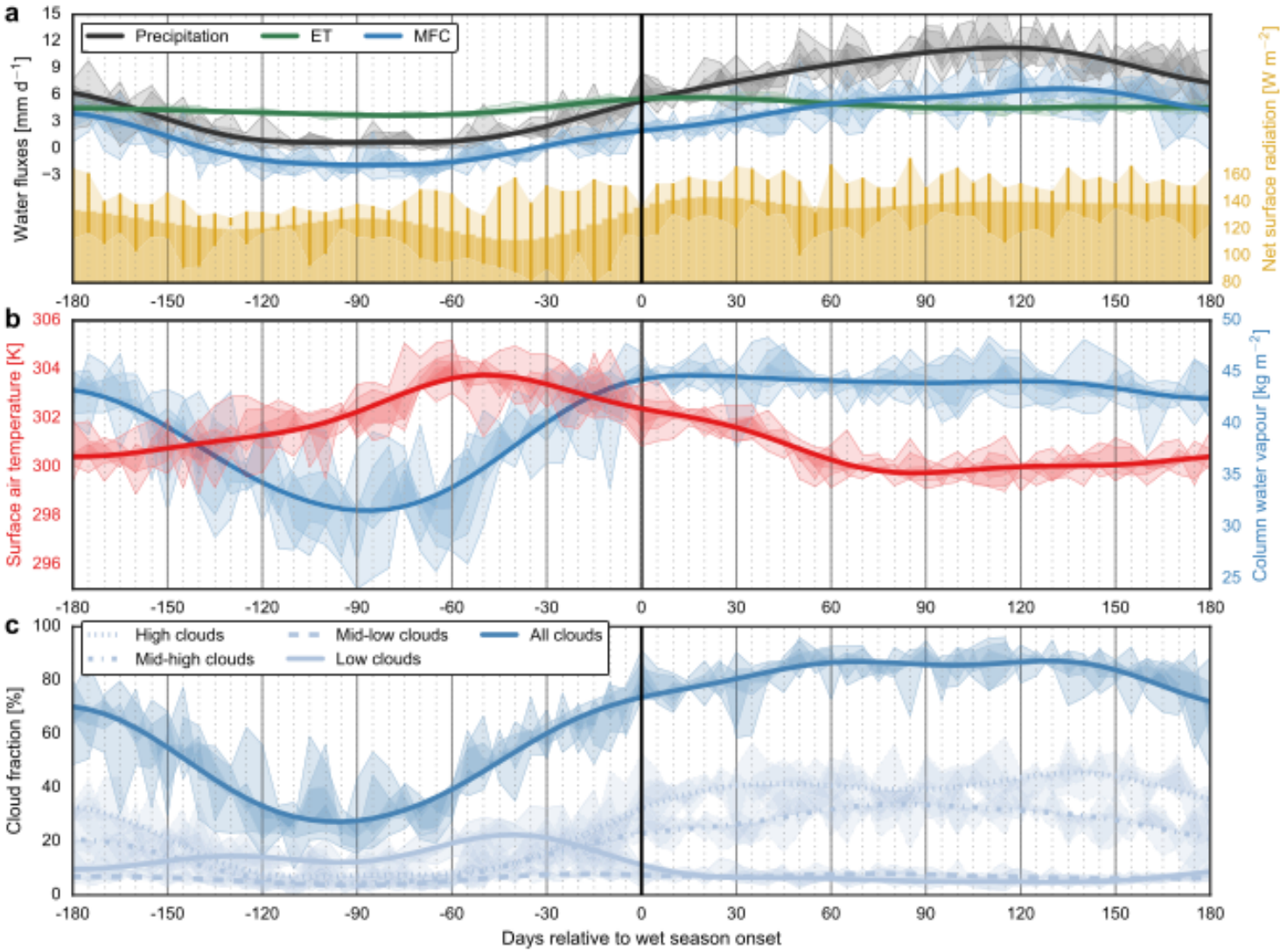

Fig. S7. Full onset-relative annual cycle of precipitation from TRMM, ET, and moisture flux convergence from ERA-Interim, and net (downward) surface radiation flux at the surface from CERES SYN1Deg (*A*), surface air temperature and CWV from AIRS (*B*), and total and vertically-resolved cloud fraction from CERES SYN1Deg (*C*). Data from individual years are shown without low-pass filtering to illustrate the scale of the unfiltered variability.

Materiais e métodos

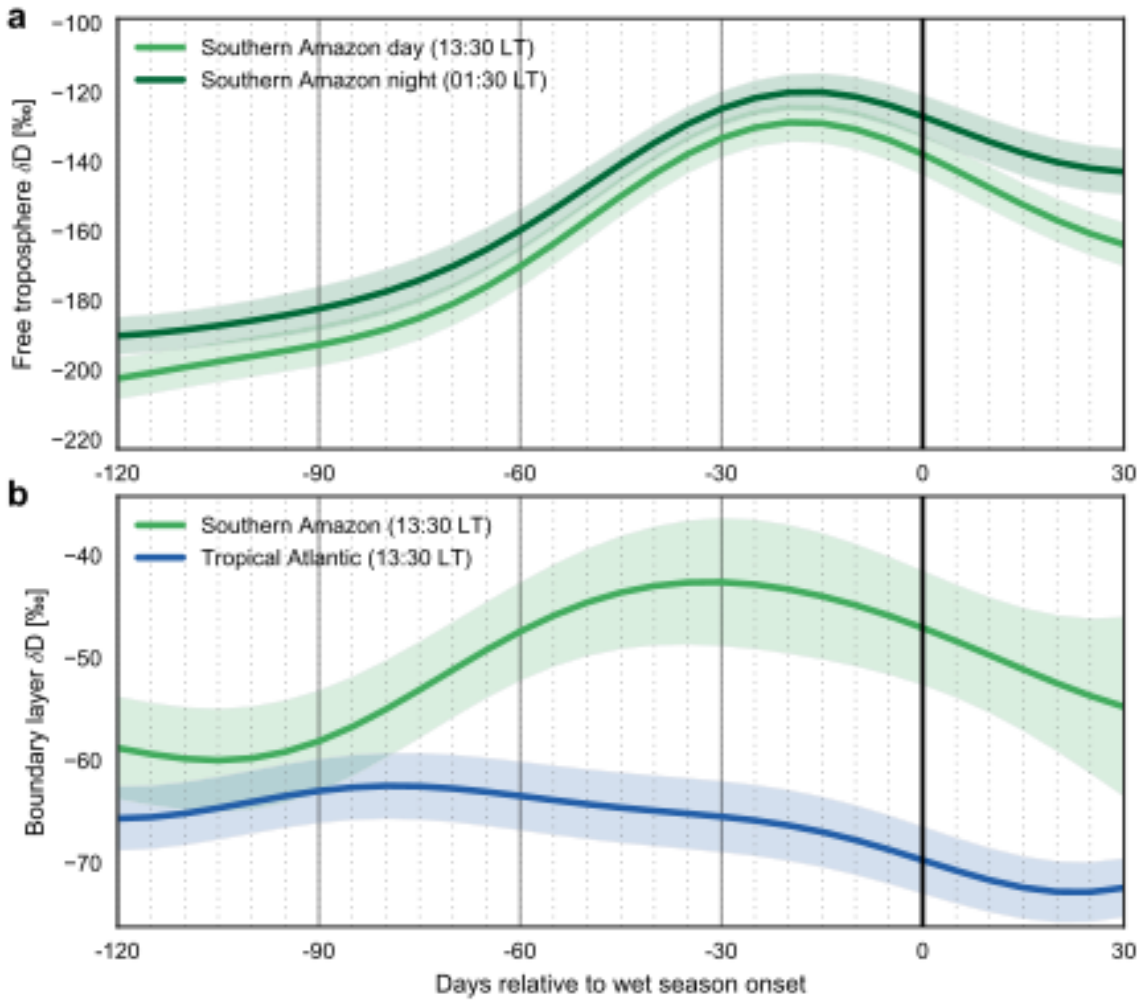

Fig. S8. Onset-relative composite time series of area-mean δD of water vapor in the free troposphere (750 to 348 hPa) (*A*) and the ABL (surface–825 hPa) (*B*) based on TES satellite retrievals from ascending (~13:30 local time) and descending (~01:30 local time) satellite overpasses. Data in *B* are shown for ascending overpasses only because TES is not sufficiently sensitive to ABL δD during descending overpasses (see also *Materials and Methods* and Fig. S9). The evolution of ABL δD over the tropical Atlantic (0–10° N, 30–55° W) is also shown for reference. Uncertainty bounds include statistical and measurement uncertainties propagated from individual TES measurements.

Materiais e métodos

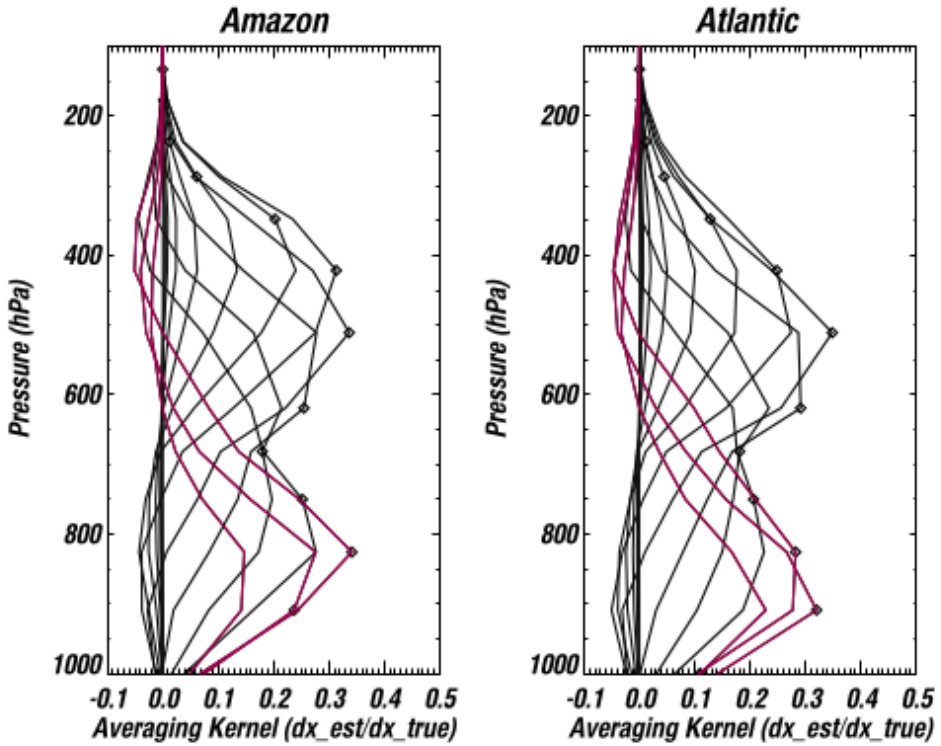

Fig. S9. Mean averaging kernels for TES observations of water vapor and HDO vapor from ascending orbits (∼13:30 local time) over the southern Amazon (*Left*) and the tropical Atlantic (*Right*) during October 2006, representative of the late dry season in the southern Amazon. Diamonds indicate pressure levels in the TES retrieval vertical grid. Averaging kernel rows for levels between the surface and 800 hPa (red lines) contribute to estimates of δD in the boundary layer (Fig. S8*B*); averaging kernel rows for levels between 800 hPa and 350 hPa contribute to estimates of δD in the free troposphere (Fig. S8*A*). The averaging kernel for descending orbits (∼01:30 local time) over the southern Amazon is similar for pressures $<$700 hPa, but sensitivity in the boundary layer is substantially reduced (the peak sensitivities of averaging kernel rows for pressures $>$800 hPa shift upward). We therefore do not consider retrievals of ABL δD (Fig. S8*B*) collected during descending passes (∼01:30 local time).

Materiais e métodos

Table S1. Wet season onset dates over the southern Amazon domain for 2005–2013, along with the data used from each dry-to-wet transition

Year	Onset pentad	Onset dates	Data
2005	56	4–8 October	All except SIF
2006	58	14–18 October	All except SIF
2007	57	9–13 October	All
2008	59	18–22 October	All
2009	58	14–18 October	All
2010	60	24–28 October	All
2011	57	9–13 October	SIF
2012	62	2–6 November	SIF
2013	57	9–13 October	SIF